Atmospheric
Chemistry
and Physics

Heterogeneity and chemical reactivity of the remote troposphere defined by aircraft measurements – corrected

Hao Guo[1], **Clare M. Flynn**[2], **Michael J. Prather**[1], **Sarah A. Strode**[3], **Stephen D. Steenrod**[3],
Louisa Emmons[4], **Forrest Lacey**[4,5], **Jean-Francois Lamarque**[4], **Arlene M. Fiore**[6], **Gus Correa**[6],
Lee T. Murray[7], **Glenn M. Wolfe**[3,8], **Jason M. St. Clair**[3,8], **Michelle Kim**[9], **John Crounse**[10],
Glenn Diskin[10], **Joshua DiGangi**[10], **Bruce C. Daube**[11,12], **Roisin Commane**[11,12], **Kathryn McKain**[13,14],
Jeff Peischl[14,15], **Thomas B. Ryerson**[13,15], **Chelsea Thompson**[13], **Thomas F. Hanisco**[3], **Donald Blake**[16],
Nicola J. Blake[16], **Eric C. Apel**[4], **Rebecca S. Hornbrook**[4], **James W. Elkins**[14], **Eric J. Hintsa**[13,14],
Fred L. Moore[13,14], **and Steven C. Wofsy**[11]

[1]Department of Earth System Science, University of California, Irvine, CA 92697, USA
[2]Department of Meteorology, Stockholm University, Stockholm, 106 91, Sweden
[3]Atmospheric Chemistry and Dynamics Laboratory, NASA Goddard Space Flight Center,
Greenbelt, MD 20771, USA
[4]Atmospheric Chemistry Observations and Modeling Laboratory, National Center for Atmospheric Research,
Boulder, CO 80301, USA
[5]Department of Mechanical Engineering, University of Colorado, Boulder, CO 80309, USA
[6]Department of Earth and Environmental Sciences and Lamont-Doherty Earth Observatory,
Columbia University, Palisades, NY 10964, USA
[7]Department of Earth and Environmental Sciences, University of Rochester, Rochester, NY 14611, USA
[8]Joint Center for Earth Systems Technology, University of Maryland, Baltimore County,
Baltimore, MD 21228, USA
[9]Department of Geological and Planetary Sciences, California Institute of Technology,
Pasadena, CA 91125, USA
[10]Atmospheric Composition, NASA Langley Research Center, Hampton, VA 23666, USA
[11]John A. Paulson School of Engineering and Applied Sciences, Harvard University,
Cambridge, MA 02138, USA
[12]Department of Earth and Planetary Sciences, Harvard University, Cambridge, MA 02138, USA
[13]Cooperative Institute for Research in Environmental Sciences, University of Colorado,
Boulder, CO 80309, USA
[14]Global Monitoring Division, Earth System Research Laboratory, NOAA, Boulder, CO 80305, USA
[15]Chemical Sciences Division, National Oceanic and Atmospheric Administration Earth System Research
Laboratory, Boulder, CO 80305, USA
[16]Department of Chemistry, University of California, Irvine, CA 92697, USA

Correspondence: Hao Guo (haog2@uci.edu) and Michael J. Prather (mprather@uci.edu)

Abstract. The NASA Atmospheric Tomography (ATom) mission built a photochemical climatology of air parcels based on in situ measurements with the NASA DC-8 aircraft along objectively planned profiling transects through the middle of the Pacific and Atlantic oceans. In this paper we present and analyze a data set of 10 s (2 km) merged and gap-filled observations of the key reactive species driving the chemical budgets of O_3 and CH_4 (O_3, CH_4, CO, H_2O, HCHO, H_2O_2, CH_3OOH, C_2H_6, higher alkanes, alkenes, aromatics, NO_x, HNO_3,

HNO$_4$, peroxyacetyl nitrate, and other organic nitrates), consisting of 146 494 distinct air parcels from ATom deployments 1 through 4. Six models calculated the O$_3$ and CH$_4$ photochemical tendencies from this modeling data stream for ATom 1. We find that 80 %–90 % of the total reactivity lies in the top 50 % of the parcels and 25 %–35 % in the top 10 %, supporting previous model-only studies that tropospheric chemistry is driven by a fraction of all the air. Surprisingly, the probability densities of species and reactivities averaged on a model scale (100 km) differ only slightly from the 2 km ATom 10 s data, indicating that much of the heterogeneity in tropospheric chemistry can be captured with current global chemistry models. Comparing the ATom reactivities over the tropical oceans with climatological statistics from six global chemistry models, we find generally good agreement with the reactivity rates for O$_3$ and CH$_4$. Models distinctly underestimate O$_3$ production below 2 km relative to the mid-troposphere, and this can be traced to lower NO$_x$ levels than observed. Attaching photochemical reactivities to measurements of chemical species allows for a richer, yet more constrained-to-what-matters, set of metrics for model evaluation. This paper presents a corrected version of the paper published under the same authors and title (sans "corrected") as https://doi.org/10.5194/acp-21-13729-2021.

Preface

While continuing our analysis of the NASA Atmospheric Tomography (ATom) data, we found several major mistakes or decision errors. The main conclusions were unchanged except those regarding production of O$_3$, but most of the numbers and many of the figures changed slightly. A corrigendum to the original 2021 paper was prepared, but the changes were extensive enough so that the *ACP* editors and the authors decided that a completely new paper should be produced and the 2021 paper withdrawn. The errors that were corrected are described in this preface and discussed at most briefly in the paper. First, we found that measurement errors in PAN and HNO$_4$ were large ($\sim$ 100 ppt), and when this occurred in the lower troposphere, the rapid thermal decomposition released large amounts of NO$_x$. There is no easy fix for this, and we developed a new protocol (reactivity data stream, RDS*) for computing reactivities by allowing the species to thermally decompose before use in the model, as described below. This fix greatly reduced O$_3$ production (P-O3) in the lower troposphere. A second NO$_x$ problem involved the propagation of polluted profiles from the Los Angeles basin to gap-filling over the tropical eastern Pacific. This correction resulted in the update of the modeling data stream to version 2b. These NO$_x$ errors cause noticeable changes in reactivities, especially P-O3. Other decision errors led us to decrease the southern latitude extent of the Atlantic and Pacific transects from 54 to 53° S to avoid spurious parcels being included. Also, cosine of latitude weighting was applied to data for all figures and tables. The UCI model now includes all higher alkanes and alkenes in the ATom data as C$_3$H$_8$ and C$_2$H$_4$, respectively. These last three decision errors had detectable but small impacts.
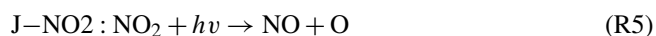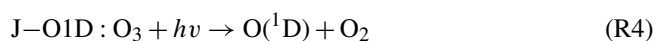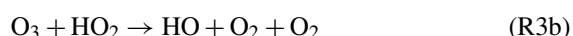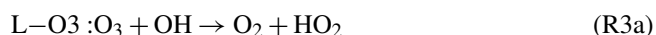
The most worrisome error was the evolution of the ATom version of the UCI Chemistry Transport Model (CTM) from its use in the MDS-0 (modeling data stream version 0) results shown here to the final calculations with MDS-2 as the UCI2* model in the 2021 paper. The first MDS-0 UCI model was taken direct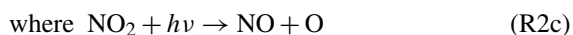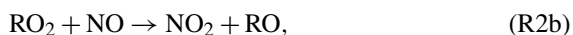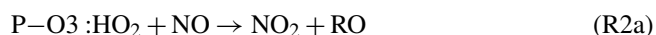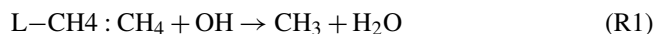ly from the main CTM code line and developed for Prather et al. (2017, 2018) by Xin Zhu (not in the 2021 paper). This model was then further adapted and developed for the 2021 paper and for additional complex sensitivity tests. At this stage (i.e., the UCI2* simulations in the 2021 paper), the results failed several logic tests and were irreproducible. With the decision to withdraw the paper, we returned to the MDS-0 UCI model, and Xin Zhu adapted it to more efficient ATom runs as well as adding several new diagnostics and checks to ascertain the ATom runs were being calculated correctly. As noted in the paper below, we carefully checked the O$_3$ budget in terms of rates and tendencies, and these are now consistent in the UCIZ (Zhu version) model. Further, the sensitivity coefficients ($\partial \ln R / \partial \ln X$ and $\partial^2 \ln R / \partial \ln X \partial \ln Y$) calculated for a subsequent paper are now closer to theoretical expectations for a quasi-linear system. The UCIZ* model results, calculated with the UCIZ CTM and the RDS* protocol, shown here are our best, revised estimate of the ATom reactivities.

1   Prologue

This paper is based on the methods and results of papers that established an approach for analyzing aircraft measurements, specifically the NASA Atmospheric Tomography Mission (ATom), with global chemistry models. Here we present a brief overview of those papers to help the reader understand the basis for this paper. The first ATom modeling paper ("Global atmospheric chemistry – which air matters", Prather et al., 2017, hence P2017) gathered six global models, both chemistry transport models (CTMs) and chemistry–climate models (CCMs). The models reported a single-day snapshot for mid-August (the time of the first ATom deployment, ATom-1), and these included all species relevant for tropospheric chemistry and the 24 h reactivities. We limited our study to three reactivities (Rs) controlling methane (CH$_4$) and tropospheric ozone (O$_3$) using specific reaction rates to define the loss of CH$_4$ and the production and loss of O$_3$ in

parts per billion (ppb) per day. The critical photolysis rates (J values) were also reported as 24 h averages.

$$L-CH4 : CH_4 + OH \rightarrow CH_3 + H_2O \qquad (R1)$$

$$P-O3 : HO_2 + NO \rightarrow NO_2 + RO \qquad (R2a)$$
$$RO_2 + NO \rightarrow NO_2 + RO, \qquad (R2b)$$
$$\text{where } NO_2 + h\nu \rightarrow NO + O \qquad (R2c)$$
$$\text{and } O + O_2 \rightarrow O_3$$
$$O_2 + h\nu \rightarrow O + O(x2) \qquad (R2d)$$

$$L-O3 : O_3 + OH \rightarrow O_2 + HO_2 \qquad (R3a)$$
$$O_3 + HO_2 \rightarrow HO + O_2 + O_2 \qquad (R3b)$$
$$O(^1D) + H_2O \rightarrow OH + OH \qquad (R3c)$$

$$J-O1D : O_3 + h\nu \rightarrow O(^1D) + O_2 \qquad (R4)$$

$$J-NO2 : NO_2 + h\nu \rightarrow NO + O \qquad (R5)$$
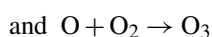
Models also reported the change in O_3 over 24 h, and these match the P-O3 minus L-O3 values over the Pacific basin (a focus of this study). The models showed a wide range in the three Rs' average profiles across latitudes over the Pacific basin, as well as 2D probability densities (PDs) for key species such as NO_x ($NO + NO_2$) versus HOOH. A large part of the model differences was attributed to the large differences found in chemical composition rather than the calculation of rates from that composition. We found that single transects from a model through the tropical Pacific at different longitudes produced nearly identical 2D PDs, but these PDs were distinctly different across models. This result supported the premise that the ATom PDs would provide a useful metric for global chemistry models.

In P2017, we established a method for running the chemistry modules in the CTMs and CCMs with an imposed chemical composition from aircraft data: the ATom run, or "A run". In the A run, the chemistry of each grid cell does not interact with its neighbors or with externally imposed emission sources. Effectively the CTM/CCM is initialized and run for 24 h without transport, scavenging, or emissions. Aerosol chemistry is also turned off in the A runs. This method allows each parcel to evolve in response to the daily cycle of photolysis in each model and be assigned a 24 h integrated reactivity. The instantaneous reaction rates at the time an air parcel is measured (e.g., near sunset at the end of a flight) do not reflect that parcel's overall contribution to the CH_4 or O_3 budget; a full diel cycle is needed. The A run assumption that parcels do not mix with neighboring air masses is an approximation, and thus for each model we compared the A runs using the model's restart data with a parallel standard 24 h simulation (including transport, scavenging, and emissions). Because the standard grid-cell air moves and mixes, we compared averages over a large region (e.g., tropical Pacific). We find some average biases of order $\pm 10\%$ but general agreement. The largest systematic biases in the A runs are caused by buildup of HOOH (no scavenging) and decay of NO_x (no sources). The A runs are relatively easy to code for most CTM/CCMs and allow each model's chemistry module, including photolysis package, to run normally. The A runs do not distinguish between CTMs and CCMs, except that each model will generate/prescribe its own cloud fields and photolysis rates. Our goal is to create a robust understanding of the chemical statistics including the reactivities with which to test and evaluate the free-running CCMs, and thus we do not try to model the specific period of the ATom deployments. Others may use the ATom data with hindcast CTMs to test forecast models, but here we want to build a chemical climatology.

The first hard test of the A runs came with the second ATom modeling paper ("How well can global chemistry models calculate the reactivity of short-lived greenhouse gases in the remote troposphere, knowing the chemical composition", Prather et al., 2018, hence P2018). The UCI CTM simulated an aircraft-like data set of 14 880 air parcels along the International Date Line from a separate high-resolution (0.5°) model. Each parcel is defined by the following core species: H_2O, O_3, NO_x, HNO_3, HNO_4, PAN (peroxyacetyl nitrate), CH_3NO_3, HOOH, CH_3OOH, HCHO, CH_3CHO (acetaldehyde), C_3H_6O (acetone), CO, CH_4, C_2H_6, alkanes (C_3H_8 and higher), C_2H_4, aromatics (benzene, toluene, and xylene), and C_5H_8 (isoprene), plus temperature. Short-lived radicals (e.g., OH, HO_2, and CH_3OO) were initialized at small concentrations and quickly reached daytime values determined by the core species. The six CTM/CCMs overwrote the chemical composition of a restart file, placing each pseudo-observation in a unique grid cell according to its latitude, longitude, and pressure. If another parcel is already in that cell, then it is shifted east–west or north–south to a neighboring model cell. For coarse-resolution models, multiple restart files and A runs were used to avoid large location shifts. CTM/CCMs usually have a locked in 24 h integration step starting at 00:00 UTC that is extremely difficult to modify in order to try to match the local solar time of observation, especially as it changes along aircraft flights. We tested the results with a recoded UCI CTM to start at 12:00 UTC but retain the same clouds fields over the day and found only percentage-level differences between a midnight or noon start.

These A runs averaged over cloud conditions by simulating 5 d in August at least 5 d apart. Assessment of the modeled photolysis rates and comparison with the ATom-measured J values is presented in Hall et al. (2018, hence

H2018). All models agreed that a small fraction of chemically hot air parcels in the synthetic data set controlled most of the total reactivity. Some models had difficulty in implementing the A runs because they overwrote the specified water vapor with the modeled value, but this problem is fixed here. In both P2017 and P2018, the GISS-E2 model stood out with the most unusual chemistry patterns and sometimes illogical correlations. Efforts by a co-author to clarify the GISS results or identify errors in the implementation have not been successful. GISS results are included here for completeness in the set of three papers but are not reconciled. Overall, three models showed remarkable inter-model agreement in the three Rs with less than half of the RMSD (root-mean-square difference) as compared with the other models. UCI also tested the effect of different model years (1997 and 2015 versus reference year 2016), which varies the cloud cover and photolysis rates, and found an inter-year RMSD about half of that of the core model's RMSD. Thus, there is a fundamental uncertainty in this approach due to the inability to specify the cloud/photolysis history seen by a parcel over 24 h, but it is less than the inter-model differences among the most similar models.

2   Introduction

The NASA Atmospheric Tomography (ATom) mission completed a four-season deployment, each deployment flying from the Arctic to Antarctic and back, traveling south through the middle of the Pacific Ocean, across the Southern Ocean, and then north through the Atlantic Ocean, with near-constant profiling of the marine troposphere from 0.2 to 12 km altitude (see Fig. S1 in the Supplement). The DC8 was equipped with in situ instruments that documented the chemical composition and conditions at time intervals ranging from < 1 to about 100 s (Wofsy et al., 2018). ATom measured hundreds of gases and aerosols, providing information on the chemical patterns and reactivity in the vast remote ocean basins, where most of the destruction of tropospheric ozone (O_3) and methane (CH_4) occurs. Reactivity is defined here as in P2017 to include the production and loss of O_3 (P-O3 and L-O3, ppb d^{-1}) and loss of CH_4 (L-CH4, ppb d^{-1}). Here we report on this model-derived product that was proposed for ATom, the daily averaged reaction rates determining the production and loss of O_3 and the loss of CH_4 for 10 s averaged air parcels. We calculate these rates with 3D chemical models that include variations in clouds and photolysis and then assemble the statistical patterns describing the heterogeneity (i.e., high spatial variability) of these rates and the underlying patterns of reactive gases.

Tropospheric O_3 and CH_4 contribute to climate warming and global air pollution (Stocker et al., 2013). Their abundances in the troposphere are controlled largely by tropospheric chemical reactions. Thus, chemistry–climate assessments seeking to understand past global change and make future projections for these greenhouse gases have focused on the average tropospheric rates of production and loss and how these reactivities are distributed in large semi-hemispheric zones throughout the troposphere (Griffiths et al., 2021; Myhre et al., 2014; Naik et al., 2013; Prather et al., 2001; Stevenson, et al., 2006, 2013, 2020; Voulgarakis et al., 2013; Young et al., 2013). The models used in these assessments disagree on these overall CH_4 and O_3 reactivities (a.k.a. the budgets), and resolving the cause of such differences is stymied because of the large number of processes involved and the resulting highly heterogeneous distribution of chemical species that drive the reactions. Simply put, the models use emissions, photochemistry, and meteorological data to generate the distribution of key species such as nitrogen oxides ($NO_x = NO + NO_2$) and hydrogen peroxide (HOOH) (step 1) and then calculate the CH_4 and O_3 reactivities from these species (step 2). There is no single average measurement that can test the verisimilitude of the models. Stratospheric studies such as Douglass et al. (1999) have provided a quantitative basis for testing chemistry and transport and defining model errors, but few of these studies have tackled the problem of modeling the heterogeneity of tropospheric chemistry. The major model differences lie in the first step because when we specify the mix of key chemical species, most models agree on the CH_4 and O_3 chemical budgets (*P2018*). The intent of ATom was to collect an atmospheric sampling of all the key species and the statistics defining their spatial variability and thus that of the reactivities of CH_4 and O_3.

Many studies have explored the ability of chemistry transport models (CTMs) to resolve finer scales such as pollution layers (Eastham and Jacob, 2017; Rastigejev et al., 2010; Tie et al., 2010; Young et al., 2018; Zhuang et al., 2018), but these have not had the chemical observations (statistics) to evaluate model performance. In a great use of chemical statistics, Yu et al. (2016) used 60 s data ($\sim$ 12 km) from the SEAC[4]RS aircraft mission to compare cumulative probability densities (PDs) of NO_x, O_3, HCHO, and isoprene over the Southeast US with the GEOS-Chem CTM run at different resolutions. They identified clear biases at the high and low ends of the distribution, providing a new test of models based on the statistics rather than mean values. Heald et al. (2011) gathered high-resolution profiling of organic and sulfate aerosols from 17 aircraft missions and calculated statistics (mean, median, and quartiles) but only compared with the modeled means. The HIAPER Pole-to-Pole Observations (HIPPO) aircraft mission (Wofsy, 2011) was a precursor to ATom with regular profiling of the mid-Pacific including high-frequency 10 s sampling that identified the small scales of variability throughout the troposphere. HIPPO measurements were limited in species, lacking O_3, NO_x, and many of the core species needed for reactivity calculations. ATom, with a full suite of reactive species and profiling through the Atlantic basin, provides a wealth of

chemical statistics that challenge the global chemistry models.

One main task here is the assembly of the modeling data stream (MDS), which provides flight-wise continuous 10 s data (air parcels) for the key reactive species. The MDS is based on direct observations and interpolation methods to fill gaps as documented in the Supplement. Using version 0 of the MDS, we have six chemical models calculating the 24 h reactivities, producing a reactivity data stream (RDS version 0) using protocols noted in the Prologue (P2017) and described further in Sect. 3.2. There, we describe the updated modeling protocol RDS* necessary to address measurement noise in PAN and HNO_4, which can be very short-lived. In Sect. 4, we examine the statistics of reactivity over the Atlantic and Pacific oceans, focusing on air parcels with high reactivity; for example, 10 % of the parcels produce 25 %–35 % of total reactivity over the oceans. We compare these ATom-1 statistics, species, and reactivities with August climatologies from six global chemistry models. In one surprising result, ATom-1 shows a more reactive tropical troposphere than found in most models' climatologies associated with higher NO_x levels than in the models. Section 5 concludes that the ATom PDs based on 10s air parcels do provide a valid chemistry metric for global models with 1° resolution. It also presents some examples where ATom measurements and modeling can test the chemical relationships and may address the cause of differences in the O_3 and CH_4 budgets currently seen across the models. With this paper we release the full ATom MDS-2b from all four deployments, along with the updated RDS-2b reactivities from the UCI model.

3 Models and data

3.1 The modeling data stream (MDS)

The ATom mission was designed to collect a multi-species, detailed chemical climatology that documents the spatial patterns of chemical heterogeneity throughout the remote troposphere. Figure S1 maps the 48 research flights, and the Supplement has tables summarizing each flight. We required a complete set of key species in each air parcel to initialize the models that calculate the CH_4 and O_3 reactivities. We choose the key reactive species (H_2O, O_3, CO, CH_4, NO_x, NO_xPSS, HNO_3, HNO_4, PAN, CH_2O, H_2O_2, CH_3OOH, acetone, acetaldehyde, C_2H_6, C_3H_8, i-C_4H_{10}, n-C_4H_{10}, alkanes, C_2H_4, alkenes, C_2H_2, C_5H_8, benzene, toluene, xylene, CH_3ONO_2, $C_2H_5ONO_2$, $RONO_2$, and CH_3OH) directly from the ATom measurements and then add corollary species or other observational data indicative of industrial or biomass burning pollution or atmospheric processing (HCN, CH_3CN, SF_6, relative humidity, aerosol surface area (four modes), and cloud indicator). We choose 10 s averages for our air parcels as a compromise and because the 10 s merged data are a standard product (Wofsy et al., 2018). A few instruments measure at 1 s intervals, but the variability at this scale is not that different from 10 s averages (Fig. S2). Most of the key species are reported as 10 s values, with some being averaged or sampled at 30 s or longer such as ~ 90 s for some flask measurements.

Throughout ATom, gaps occur in individual species on a range of timescales due to calibration cycles, sampling rates, or instrument malfunction. The generation of the MDS uses a range of methods to fill these gaps and assigns a flag index to each species and data point to allow users to identify direct measurements and methods used for gap-filling. Where two instruments measure the same species, the MDS selects a primary measurement and identifies which instrument was used with a flag. The methodology and species-specific information on how the current MDS version 2 (MDS-2) is constructed, plus statistics on the 48 research flights and the 146 494 10 s air parcels in MDS-2, are given in the Supplement.

Over the course of this study, several MDS versions were developed and tested, including model-derived RDSs from these versions, some of which are used in this paper. In early ATom science team meetings, there was concern about the accuracy of NO_2 direct measurements when at very low concentrations. A group prepared an estimate for NO_x using the NO and O_3 measurements to calculate a photostationary value for NO_2 and thus NO_x. This PSS-NO_x became the primary NO_x source in version 0 (i.e., MDS-0). With MDS-0, we chose to gap-fill using correlations with CO to estimate the variability of the missing measurement over the gap. The science team then rejected PSS-NO_x as a proxy, and we reverted to the observed NO + NO_2 resulting in NO_x values that are 25 % larger on average than in MDS-0 (unweighted mean of 66 vs. 52 ppt). This change affected P-O3 most and L-CH4 least. We then estimated errors in the gap-filling and found that CO had little skill as a proxy for most other species. With MDS-2, we optimized and tested the treatments of gap-filling and lower limit of detection, along with other quality controls. With continued analysis of the unusually reactive eastern Pacific region, we determined that the method of long-gap filling for NO_x resulted in propagation of high NO_x levels from the over-land profiles into the over-water profiles in the tropics. We separated these two set of profiles used for long-gap NO_x filling and created an updated version 2b. This experience points to the importance of having reliable, continuous NO_x measurements. MDS-2b is fully documented in the Supplement.

3.2 The reactivity data stream (RDS)

The concept of using an MDS to initialize 3D global chemistry models and calculate an RDS was developed in the pre-ATom methodology papers (P2017; P2018). In this paper, we use the original six models for their August chemical statistics, and we use five of them plus a box model to calculate the reactivities; see Table 1. The RDS is really a protocol applied to the MDS. It is introduced in the Prologue, and the details can be found in P2018. A model grid cell chosen to be close

Table 1. Chemistry models.

Used for	ID	Model name	Model type	Meteorology	Model grid
clim	GFDL	GFDL-AM3	CCM	NCEP (nudged)	$C180 \times L48$
clim, MDS-0	GISS	GISS-E2.1	CCM	Daily SSTs, nudged to MERRA	$2° \times 2.5° \times 40L$
clim, MDS-0	GMI	GMI-CTM	CTM	MERRA	$1° \times 1.25° \times 72L$
clim, MDS-0	GC	GEOS-Chem	CTM	MERRA-2	$2° \times 2.5° \times 72L$
clim, MDS-0	NCAR	CAM4-Chem	CCM	Nudged to MERRA	$0.47° \times 0.625° \times 52L$
clim, MDS-0 & 2b	UCI	UCI-CTM	CTM	ECMWF IFS Cy38r1	$T159N80 \times L60$
MDS-0	F0AM	F0AM	box	MDS + scaled ATom Js	n/a

The descriptions of models used in the paper. The first column denotes if the model's August climatology is used ("clim") and also the MDS versions used. F0AM used chemical mechanism MCMv331 plus J-HNO$_4$ plus O^{1}D) + CH$_4$. For the global models, see P2017, P2017, and H2018. n/a – not applicable.

Table 2. Reactivity statistics for the three large domains (global, Pacific, and Atlantic).

		Models using MDS-0								MDS-2b
Value	Region	F0AM	GC	GISS	GMI	NCAR	UCI	U15	U97	UCIZ*
P-O3, mean, ppb d^{-1}	Global	2.12	2.12	2.57	2.08	2.22	2.38	2.37	2.37	1.23
	Pacific	1.96	2.00	1.99	1.96	2.01	2.17	2.13	2.15	1.11
	Atlantic	1.96	2.12	3.49	2.20	2.44	2.48	2.48	2.49	1.25
L-O3, mean, ppb d^{-1}	Global	1.81	1.63	1.93	1.70	1.76	1.76	1.74	1.75	1.61
	Pacific	1.65	1.51	1.79	1.55	1.52	1.58	1.53	1.56	1.42
	Atlantic	2.15	2.02	2.37	2.17	2.47	2.28	2.28	2.30	2.12
L-CH4, mean, ppb d^{-1}	Global	0.81	0.76	0.43	0.75	0.73	0.79	0.78	0.78	0.61
	Pacific	0.85	0.82	0.40	0.80	0.79	0.82	0.80	0.81	0.63
	Atlantic	0.80	0.78	0.51	0.81	0.86	0.85	0.85	0.85	0.69
P-O3, % of total R in top 10 %	Global	35 %	32 %	31 %	32 %	30 %	34 %	34 %	34 %	33 %
	Pacific	34 %	28 %	28 %	29 %	29 %	30 %	30 %	30 %	27 %
	Atlantic	24 %	25 %	24 %	26 %	24 %	27 %	27 %	28 %	27 %
L-O3, % of total R in top 10 %	Global	35 %	35 %	33 %	35 %	36 %	36 %	36 %	36 %	36 %
	Pacific	33 %	32 %	29 %	32 %	31 %	32 %	32 %	32 %	32 %
	Atlantic	28 %	30 %	29 %	30 %	34 %	30 %	30 %	30 %	29 %
L-CH4, % of total R in top 10 %	Global	33 %	30 %	27 %	31 %	31 %	32 %	32 %	32 %	30 %
	Pacific	32 %	28 %	26 %	29 %	29 %	29 %	29 %	29 %	27 %
	Atlantic	27 %	25 %	21 %	26 %	27 %	27 %	27 %	27 %	25 %

Global includes all ATom-1 parcels, Pacific considers all measurements over the Pacific Ocean from 53° S to 60° N, and Atlantic uses parcels from 53° S to 60° N over the Atlantic Ocean. All parcels are weighted inversely by the number of parcels in each 10° latitude by 100 hPa bin and by cosine(latitude). Results from MDS-0 are shown because we have results from six models. Results from the updated MDS-2b are shown (UCIZ*) using the using the current UCI CTM model UCIZ and the RDS* protocol that preprocesses the MDS-2b initializations with a 24 h decay of HNO4 and PAN according to their local thermal decomposition frequencies; see text. See additional statistics in Table S8.

to the measured parcel is initialized with all the core reactive species needed for a regular chemistry simulation. The model is then integrated over 24 h without transport or mixing, without scavenging, and without emissions. Each global model uses its own varying cloud fields for the period to calculate photolysis rates, but the F0AM box model simply takes the instant J values as measured on the flight and applies a diurnal scaling. We initialize with the core species and let the radicals (OH, HO$_2$, and RO$_2$) come quickly into photochemical balance. The 24 h integration is not overly sensitive to the start time of the integration, and thus models do not have to

synchronize with the local time of observation (see P2018's Fig. S8 and Table S8).

The initial ATom-1 reactivities came from MDS-0 and six of the models in Table 1. Although these RDS-0 model results are now out of date because of the move to MDS-2b, they provide critical information on how models agree, or disagree, in calculating the RDS using the ATom protocol. Thus we include them here as a cross-model comparison. Given the excellent agreement at the parcel level using three models (GC, GMI, and UCI), and with a desire to avoid wasting the community's time, we continued the analysis of

Table 3. Cross-model rms differences (RMSDs as a percentage of the mean) for the three reactivities using MDS-0.

P-O3	F0AM	GC	GISS	GMI	NCAR	UCI
F0AM		48 %	95 %	45 %	55 %	42 %
GC	48 %		78 %	**26 %**	42 %	**32 %**
GISS	95 %	78 %		81 %	72 %	75 %
GMI	45 %	**26 %**	81 %		40 %	**35 %**
NCAR	55 %	42 %	72 %	40 %		42 %
UCI	42 %	**32 %**	75 %	**35 %**	42 %	(10 %)
L-O3						
F0AM		40 %	44 %	43 %	76 %	38 %
GC	40 %		33 %	**25 %**	60 %	**24 %**
GISS	44 %	33 %		36 %	66 %	30 %
GMI	43 %	**25 %**	36 %		62 %	**28 %**
NCAR	76 %	60 %	66 %	62 %		60 %
UCI	38 %	**24 %**	30 %	**28 %**	60 %	(11 %)
L-CH4						
F0AM		47 %	136 %	48 %	82 %	45 %
GC	47 %		111 %	**20 %**	60 %	**27 %**
GISS	136 %	111 %		114 %	110 %	121 %
GMI	48 %	**20 %**	114 %		57 %	**30 %**
NCAR	82 %	60 %	110 %	57 %		68 %
UCI	45 %	**27 %**	121 %	**30 %**	68 %	(14 %)

Matrices are symmetric. Calculated with the 31 376 MDS-0 unweighted ATom-1 parcels using the standard RDS protocol. F0AM lacks 5510 of these parcels because there are no reported J values. UCI shows RMSD between years 2016 (default) and 1997 as the value in parentheses on the diagonal. The unweighted mean R from three core models (GC, GMI, and UCI) are P-O3 = 1.97, L-O3 = 1.50, and L-CH4 = 0.66 (all ppb d^{-1}). The three core-model RMSDs with respect to one another are less than 36 % and given in bold.

MDS-2b with just our local UCI CTM. This decision may need to be revisited.

Statistics for the three reactivities for six models using MDS-0 are given in Tables 2 and S8 for three domains: global (all points), Pacific (oceanic data from 53° S to 60° N), and Atlantic (same constraints as Pacific). The statistics try to achieve equal latitude-by-pressure sampling by weighting each ATom parcel inversely according to the number of parcels in each 10° latitude by 100 hPa bin, and each point is also cosine (latitude)-weighted. We calculate the means and medians plus the percent of total reactivity in the top 10 % of the weighted parcels (Table 2) and also the mean reactivity of the top 10 %, percent of total reactivity in the top 50 %, 10 %, and 3 %, plus the mean J values (Table S8).

These six-model version 0 statistics are shown alongside the version 2b results using the current UCIZ model but with a new protocol designated RDS*. While investigating sensitivities in the RDS, we found an inconsistency between the reported concentrations of both pernitric acid (HNO$_4$) and peroxyacetyl nitrate (PAN) with respect to the chemical kinetics used in the models. High concentrations (100 ppt, attributed to instrument noise) were reported under conditions where the thermal decomposition frequency was > 0.4 per hour in the lower troposphere (> 253 K for HNO$_4$ and > 291 K for PAN). Thus, these species instantly become

NO$_x$. While these measurements are clearly spurious, there is no easy fix. We developed a new protocol, RDS*, that allows both species to decay for 24 h using their local thermal decomposition rate before being used in the model. This protocol avoids much of the fast thermal release of NO$_x$ in the lower atmosphere during the first 24 h of the RDS calculation but does not affect the release of NO$_x$ from photolysis or OH reactions in the upper troposphere where thermal decomposition is inconsequential. It is possible that some of the high concentrations of HNO$_4$ and PAN in the lower troposphere are real and that we are missing this large source of NO$_x$ with the RDS* protocol, but we find no obvious sources of these species in the remote oceanic regions that would produce enough to match the thermal loss. Both this problem and its solution do not affect the initial NO$_x$ values.

We present the RDS-2b reactivities calculated under the RDS* protocol with the UCI CTM developed by Xin Zhu for P2017 and P2018 (designated UCIZ*) as our best results in the final column of Tables 2 and S8. We added diagnostics that give us confidence in our O$_3$ reactivities: the approximate P-O3 and L-O3 based on the limited Reactions (rates 2a, b, and d and 3a, b, and c above) actually predict the calculated 24 h O$_3$ tendency; see Fig. S6. Considering the ocean basin observations only, P − L (production minus loss) ranges from −12 to +15 ppb d^{-1}. The mean error in P–L is about −0.01 ppb d^{-1}, and the root-mean-squared error is about 0.04 ppb d^{-1}, convincing us that we have correctly diagnosed the P-O3 and L-O3 terms. Following the practice of the GMI model, we also record the initial and 24 h abundances of all the ATom species to check that nothing unusual altered the species abundance in each cell over the 24 h.

3.3 Inter-model differences

Variations in reactivities due to clouds are an irreducible source of uncertainty: predicting the cloud-driven photolysis rates that a shearing air parcel will experience over 24 h is not possible here. The protocol uses 5 separated 24 h days to average over synoptically varying cloud conditions. The standard deviation (σ) of the 5 d, as a percentage of the 5 d mean, is averaged over all parcels and shown in Table S9 for the five global models. Three central models (GC, GMI, and UCI) show 9 %–10 % σ (Js) values and similar σ (Rs) values as expected if the variation in J values is driving the reactivities. Two models (GISS and NCAR) have 12 %–17 % σ (Js), which might be explained by more opaque clouds, but the amplified $\sigma(R)$ values (14 %–32 %) are inexplicable. This discrepancy needs to be resolved before using these two models for ATom RDS analysis.

Inter-model differences are shown in the parcel-by-parcel root-mean-square (rms) differences for RDS-0 in Table 3. Even when models adopt standard kinetic rates and cross sections (i.e., Burkholder et al., 2015), the number of species and chemical mechanisms included, as well as the treatment of families of similar species or intermediate short-lived reac-

Table 4. ATom data files used here.

Primary aircraft data	Formatting and content	Comments
(a) Mor.all.at1234.2020-05-27.tbl (b) Mor.WAS.all.at1234.2020-05-27.tbl (c) Mor.TOGA.all.at1234.2020-05-27.tbl All from Wofsy et al. (2018).	(a) 149 133 records × 675 csv columns, 10 s merges of flight data plus chemistry & environmental measurements (b) 6991 records × 729 csv columns, 30–120 s intervals to fill flasks (c) 12 168 records × 727 csv columns, 35 s intervals of instrument	Core source of ATom measurements. Irregular and difficult formatting, extremely long asci records, large negative integers or "NA" for some non-data.
Modeling data stream (MDS-2b)		
(a) ATom_MDS2b.nc	(a) netCDF file containing regularly spaced 10 s observations for ATom-1 (32 383 records), ATom-2 (33 424 records), ATom-3 (40 176 records), and ATom-4 (40 511 records), 146 494 in total. Includes physical flight data (11), chemical data (39), miscellaneous data including corrected HNO_4 and PAN (6), and flag data (50).	Regular formatting; all data gap-filled with flags to identify the method and extent of filling; NaN's only for flight 46; for use in modeling of the chemistry and related statistics from the ATom 10 s data.
Reactivity data stream (RDS-2b)		
(a) ATom_RDS2b.nc	(a) netCDF file containing regularly spaced reactivities for 10 s parcels from ATom-1234 (146 494 in total). Includes latitude, longitude, and pressure of model grid cell used in the calculation. Includes P-O3, L-O3, L-CH4, L-CO, and J-O1D, plus dO_3/dt = net O_3 change over 24 h. Reactivities are given for 5 d separated by 5 d in the middle of each deployment, plus the 5 d mean.	Results from newest UCI CTM version (UCIZ) run with RDS* protocol (PAN and HNO_4 decay) and using MDS-2b. NaN's only for flight 46.

tion products, varies across models. For example, UCI considers about 32 reactive gases, whereas GC and GMI have over 100, and F0AM has more than 600. The other major difference across models is photolysis, with models having different cloud data and different methods for calculating photolysis rates in cloudy atmospheres (H2018). The three central models (GC, GMI, and UCI) in terms of their 5 d variability (Table S9) are also most closely alike in these statistics, with rms = 20 %–30 % for L-CH4 up to 26 %–35 % for P-O3. These rms values appear to be about as close as any two models can get. The intra-model rms for different years (UCI 2016 versus 1997) is 10 %–13 % and shows that we are seeing basic differences in the chemical models across GC, GMI, and UCI. F0AM is the next closest to these central models, but it will inherently have a larger rms because it is a 1 d calculation and not a 5 d average. NCAR's rms is consistently higher and likely related to what is seen in the 5 d σ values in Table S9. GISS is clearly different from all the others (L-CH4 rms > 100 %, while L-O3 rms < 66 %).

4 Results

Our analysis of the reactivities uses the six-model RDS-0 results to examine the consistency in calculating the Rs across

models. Thereafter, we rely on the similar results from the three central models (GC, GMI, and UCI) to justify use of UCIZ* with MDS-2b as our best estimate for ATom reactivities. The uncertainty in this estimate can be approximated by the inter-model spread of the central models as discussed above. When evaluating the model climatologies for chemical species, we use MDS-2b. A summary of the key data files used here, as well as their sources and contents, is given in Table 4.

4.1 Probability densities of the reactivities

The reactivities for three large domains (global, Pacific, and Atlantic) from the six-model RDS-0 are summarized in Tables 2 and S8. Sorted PDs for the three Rs and Pacific and Atlantic Ocean basins are plotted in Fig. 1 and show the importance of the most reactive "hot" parcels with deeply convex curves and the sharp upturn in R values above 0.9 cumulative weight (top 10 %). Both basins show a similar emphasis on the most reactive hot parcels: 80 %–90 % of total R is in the top 50 % of the parcels, 25 %–35 % is in the top 10 %, and about 10 %–14 % is in the top 3 %. The corollary is that the bottom 50 % parcels control only 10 %–20 % of the to-

tal reactivity, which is why the median is less than the mean (except for P-O3 in the Atlantic).

The enhancement factor for the top 50 % L-CH4 parcels is 2.0 (84 % of reactivity in 42 % of mass) given that our 53° S–60° N transects cover 83 % of the air mass below 200 hPa and assuming that L-CH4 is negligible poleward of these transects. This enhancement factor is a large-scale feature because the tropical lower troposphere, being warm and wet with high sun, dominates the budget. It is seen in previous model intercomparisons that calculate budgets in large tropospheric blocks like Voulgarakis et al. (2013) with 63 % of L-CH4 in 31 % of the air mass (500 hPa–surface, 30° S–30° N). The impact of the extremely hot parcels and the heterogeneity seen in the ATom 10 s parcels is evident in the steep slopes above the 90th percentile, yielding enhancement factors of 3 to 4.

Each R value and each ocean has a unique shape; for example L-O3 in the Atlantic is almost two straight lines breaking at the 50th percentile. In Fig. 1 the agreement across all models (except GISS) is clear, indicating that the conclusion in *P2018* (i.e., that most global chemistry models agree on the O3 and CH4 budgets if given the chemical composition) also holds for the ATom-measured chemical composition. Comparing the dashed brown (UCI, RDS-0) and black (UCIZ, RDS*-2) lines, we find that the shift from MDS-0 to MDS-2b plus the new RDS* ($HNO_4 + PAN$) protocol produces large reductions in P-O3 for all cumulative weights and small reductions in L-CH4 for the upper 5th percentile. We conclude that accurate modeling of chemical composition of the 80th and greater percentiles is important but that modest errors in the lowest 50th percentile are inconsequential; effectively, some parcels matter more than others (P2017).

How well does this ATom analysis work as a model intercomparison project? Overall, we find that most models give similar results when presented with the ATom-1 MDS. The broad agreement of the cumulative reactive PDs across a range of model formulations using differing levels of chemical complexity shows this approach is robust. The different protocols for calculating reactivities as well as the uncertainty in cloud fields appear to have a small impact on the shape of the cumulative PDs but are informative regarding the minimum structural uncertainty in estimating the 24 h reactivity of a well-measured air parcel.

4.2 Spatial heterogeneity of tropospheric chemistry

A critical unknown for tropospheric chemistry modeling is what resolution is needed to correctly calculate the budgets of key gases. A similar question was addressed in Yu et al. (2016) for the isoprene oxidation pathways using a model with variable resolution (500, 250, and 30 km) compared to aircraft measurements; see also ship plume chemistry in Charlton-Perez et al. (2009). ATom's 10 s air parcels measure 2 km (horizontal) by 80 m (vertical) during most profiles. There are obviously some chemical structures below the

10 s air parcels. Only some ATom measurements are archived at 1 Hz, and we examine a test case using 1 s data for O3 and H2O for a mid-ocean descent between Anchorage and Kona in Fig. S2a. Some of the 1 s (200 m by 8 m) variability is clearly lost with 10 s averaging, but 10 s averaging preserves most of the variability. Lines in Fig. S2 demark 400 m in altitude, and most of the variability occurs on this larger, model-resolved scale. Figure S2b shows the 10 s reactivities during that descent and also indicates that much of the variability occurs at 400 m vertical scales. A more quantitative example using all the tropical ATom reactivities is shown in comparisons with probability densities below (Fig. 5).

How important is it for the models to represent the extremes of reactivity? While the sorted reactivity curves (Fig. 1, Tables 2 and S8) continue to steepen from the 90th to 97th percentile, the slope does not change that much. Thus we can estimate the 99th + percentile contributes < 5 % of the total reactivity. Thus, if our model misses the top 1 % of reactive air parcels (e.g., due to the inability to simulate intensely reactive thin pollution layers) then we miss at most 5 % of the total reactivity. This finding is new and encouraging, and it needs to be verified with the ATom-2, 3, and 4 data.

The spatial structures and variability of reactivity as sampled by the ATom tropical transects (central Pacific, eastern Pacific, and Atlantic) are presented as nine panels in Fig. 2. Here, the UCIZ RDS*-2 reactivities are averaged and plotted in 1° latitude by 200 m thick cells, comparable to some global models (e.g., GMI, NCAR, and UCI). We separate the eastern Pacific (121° W, research flight (RF) 1) from the central Pacific (RFs 3, 4, and 5) because we are looking for contiguous latitude-by-pressure structures.

In the central Pacific (Fig. 2a, d, g), highly reactive (hot) P-O3 parcels ($> 6\,ppb\,d^{-1}$) occur in larger, connected air masses at latitudes 20–22° N and pressure altitudes 2–3 km and in more scattered parcels ($> 3\,ppb\,d^{-1}$) below 5 km down to 20° S. High L-O3 and L-CH4 coincide with this 20–22° N air mass and also with some high P-O3 at lower latitudes. This pattern of overlapping extremes in all three Rs is surprising because the models' mid-Pacific climatologies show a separation between regions of high L-O3 (lower–middle troposphere) and high P-O3 (upper troposphere, as seen in P2017's Fig. 3). The obvious explanation is that the models leave most of the lightning-produced NO_x in the upper troposphere. The ATom profiling seems to catch reactive regions in adjacent profiles separate by a few hundred kilometers, scales easily resolvable with 3D models.

In the eastern Pacific (Fig. 2b, e, h), the overlap of outbound and return profiles enhances the spatial sampling over the 10 h flight. The region of very large L-O3 ($> 5\,ppb\,d^{-1}$) is extensive, beginning at 5–6 km at 10° N and broadening to 2–8 km at 28° N. The region of L-CH4 is similar, but loss at the upper altitudes of this air mass is attenuated because of the temperature dependence of L-CH4 and possibly because of differing OH : HO2 ratios with altitude. Large P-O3
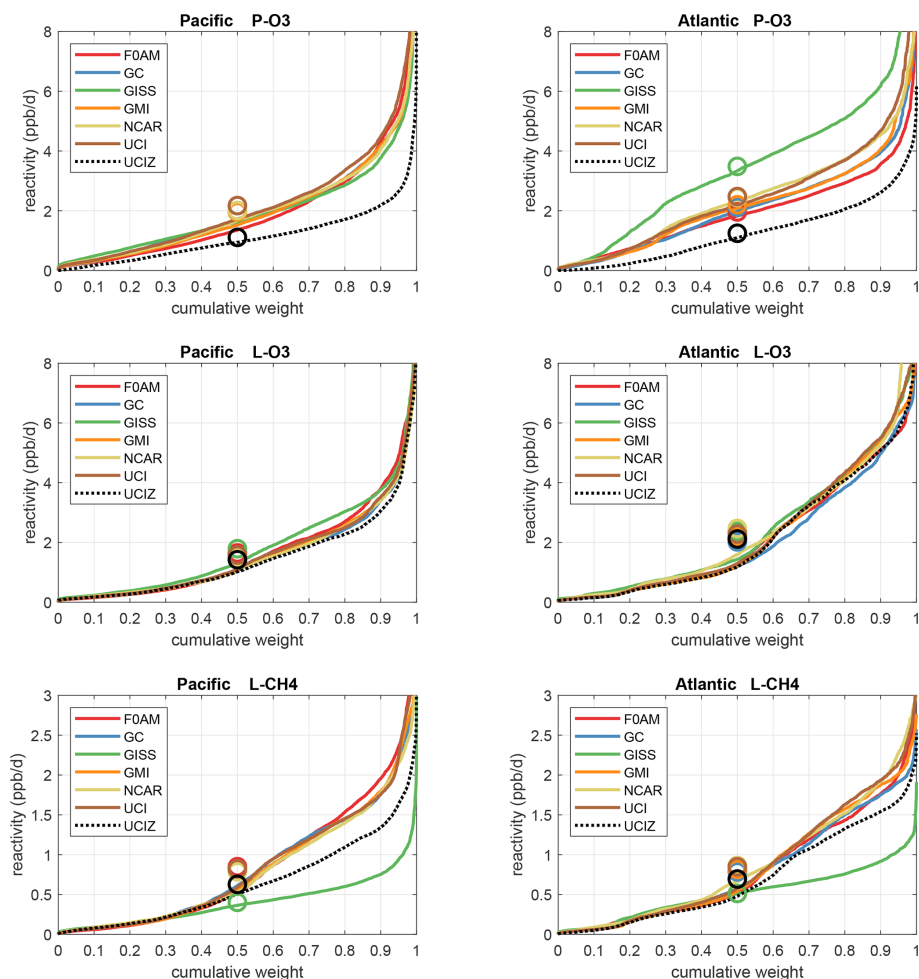
Figure 1. Sorted reactivities (P-O3, L-O3, and L-CH4, in $ppb\,d^{-1}$; three successive rows) for the Pacific and Atlantic domains (53° S–60° N, two columns) of ATom-1. Each parcel is weighted, including cosine (latitude); see text. Results from six models using MDS-0 and the standard RDS protocol are shown with colored lines; the updated UCIZ CTM using MDS-2b with the RDS* protocol (HNO4 and PAN damping) is shown as a dashed black line. The mean value for each model is shown with an open circle plotted at the 50th percentile. (Flipped about the axes, this is a cumulative probability density function.)

($> 3\,ppb\,d^{-1}$) occurs only in the center of this highly reactive L-O3/L-CH4 region, suggesting that NO_x is not as evenly distributed as HO_x is. Highly reactive (hot) P-O3 parcels ($> 4\,ppb\,d^{-1}$) occur only in the upper troposphere (8–12 km) and only in the sub-tropics. ATom-1 RF1 (29 July 2016) occurred during the North American Monsoon when there was easterly flow off Mexico; thus the high reactivity of this large air mass indicates that continental deep convection with lightning NO_x is a source of high reactivity for both O_3 and CH_4.

In the Atlantic (Fig. 2c, f, i), we also see similar air masses through successive profiles, particularly in the northern tropics. The Atlantic P-O3 shows high-altitude reactivity similar to the eastern Pacific. Likewise, the large values of L-O3 and L-CH4 match the eastern Pacific and not the central Pacific. Unlike either Pacific transect, the Atlantic L-O3 and L-CH4 show some high reactivity below 1 km altitude. Overall, the

ATom-1 profiling clearly identifies extended air masses of high L-O3 and L-CH4 extending over 2–5 km in altitude and 10° of latitude. The high P-O3 regions tend to be much more heterogeneous with greatly reduced spatial extent, likely of recent convective origin as for the eastern Pacific.

Overall, the extensive ATom profiling identifies a heterogeneous mix of chemical composition in the tropical Atlantic and Pacific, with a large range of reactivities. What is important for those trying to model tropospheric chemistry is that the spatial scales of variability seen in Fig. 2 should be within the capability of modern global models.

4.3 Testing model climatologies

The ATom data set provides a unique opportunity to test CTMs and CCMs in a climatological sense. In this section, we compare ATom-1 data and the six models' chemical
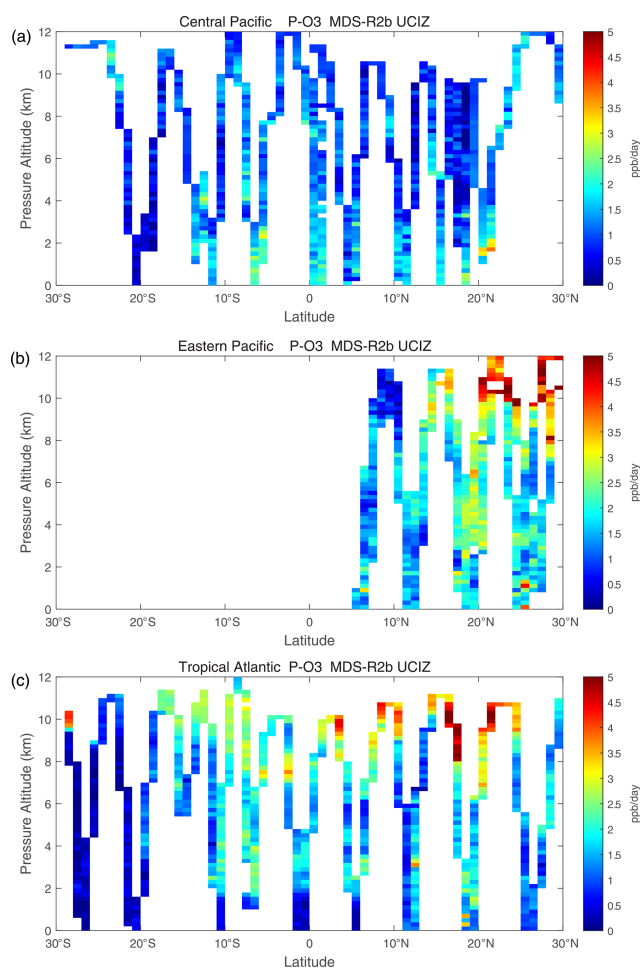
Figure 2.

Figure 2.

statistics for mid-August used in P2017. The ATom profiles cannot be easily compared point by point with CCMs, and we use statistical measures of the three reactivities in the three tropical basins: mean profiles in Fig. 3 and PDs in Fig. 5.

4.3.1 Profiles

For P-O3 profiles (top row, Fig. 3), the agreement between models and measurements is passable except for the 0–2 km region in both the central and eastern Pacific, where the models fail to predict the observed 2 ppb d^{-1} O$_3$ production. In the central Pacific at 3–12 km, ATom-1 results agree with models, showing ozone production of about 1 ppb d^{-1}. In the eastern Pacific and Atlantic at 3–12 km, ATom-1 results also agree with models but at a higher ozone production of about 2 ppb d^{-1}. This pattern indicates that in the central Pacific, the NO$_x$ + HO$_x$ combination that produces ozone is suppressed below 2 km in all the models. In the upper troposphere, 10–12 km, of the eastern Pacific and Atlantic, ATom P-O3 values show a jump to 3 ppb d^{-1}, which is only partly reproduced in the models. We take this pattern as evidence
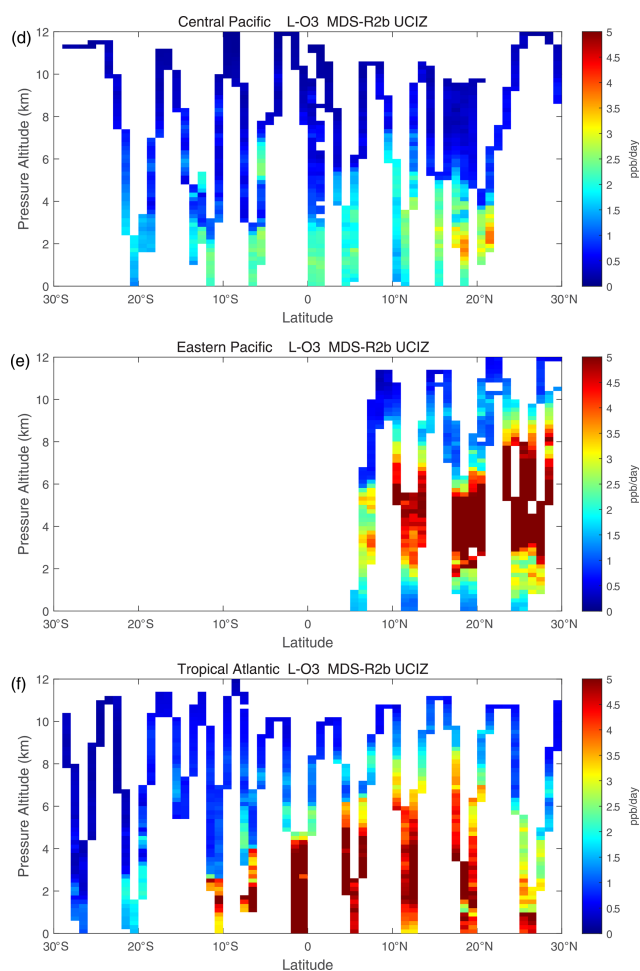
for lightning NO$_x$ production and export over the adjacent continents.

For L-O3 (middle row, Fig. 3) in the central Pacific, ATom-1 results match the throughout the 0–12 km range (except GISS). Moving to the eastern Pacific and Atlantic, most models show a mid-level peak above 2 km, while ATom-1 shows an even larger peak for L-O3, especially in the eastern Pacific at 3–6 km where L-O3 > 4 ppb d^{-1}. This mid-tropospheric peak is evident in the curtain plots of Fig. 2 and likely due to easterly mid-tropospheric flow from convection over Mexico at that specific time (29 July 2016). Similarly, the ATom re-activity at 1–3 km in the Atlantic is associated with biomass burning in Africa and was measured in other trace species. Thus, in terms of L-O3, the ATom–model differences may be due to specific meteorological conditions, and this could be tested with CTMs using 2016 meteorology and wildfires.

For L-CH4 (bottom row, Fig. 3), the ATom–model patterns are similar to L-O3, including the large ATom-only losses (> 1.5 ppb d^{-1} over 3–6 km) in the eastern Pacific but with higher reactivities occurring at slightly lower altitudes be-cause of the large negative temperature dependence of Reac-
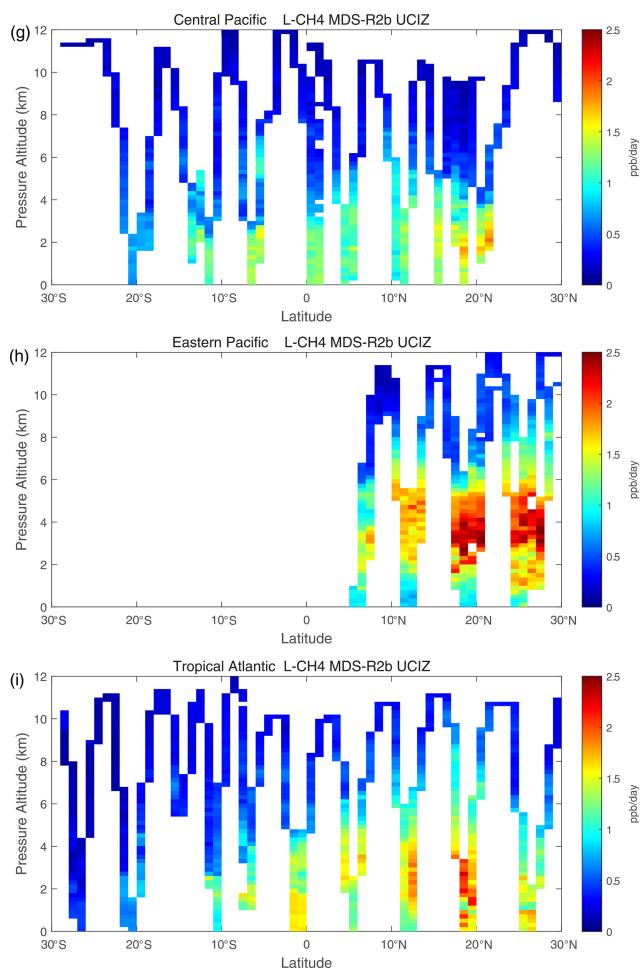
Figure 2. Curtain plots for P-O3 (0–5 ppb d^{-1}; panels **a, b, c**), L-O3 (0–5 ppb d^{-1}; panels **d, e, f**), and L-CH4 (0–2.5 ppb d^{-1}; panels **g, h, i**) showing the profiling of ATom-1 flights in the central Pacific (RF 3, 4 and 5; panels **a, d, g**), eastern Pacific (RF 1; panels **b, e, h**), and Atlantic (RF 7, 8, and 9; panels **c, f, i**). Reactivities are calculated with the current UCIZ CTM model using MDS-2b and the RDS* protocol; see text. The 10 s air parcels are averaged into 1° latitude and 200 m altitude bins.

tion (1). L-O3 is dominated by O(1D) and HO$_2$ loss, while L-CH4 is limited to OH loss. Overall, there is clear evidence that the Atlantic and Pacific have very different chemical mixtures controlling the reactivities and that convection over land (monsoon or biomass burning) creates air masses that are still highly reactive a day or so later.

4.3.2 Key species

The deficit in modeled P-O3 in the central and eastern Pacific at 0–2 km altitude points to a NO$_x$ deficiency in the models, and this becomes obvious in the comparison of the PD histograms for NO$_x$ shown in Fig. 4. Over 0–12 km (first row), ATom has a reduced frequency of parcels with 1–10 ppt and a corresponding increase in parcels with 20-60 ppt; this dis-

crepancy is amplified in the lower troposphere, 0–4 km (second row). The obvious source of this oceanic NO$_x$ is lightning since oceanic sources of organonitrates or other nitrate species measured on ATom could not supply this amount. The ATom statistics indicate such a lightning source must be mixed down into the boundary layer. In the eastern Pacific and Atlantic, the full troposphere PD more closely matches the models, including a bump in 100–300 ppt NO$_x$ which is probably direct outflow from very deep convection with lightning over the neighboring continents. Overall, the models appear to be missing significant NO$_x$ sources in all three regions below 4 km.

In Fig. 4, we also look at the histograms for the key HO$_x$-related species HOOH (third row) and HCHO (fourth row). For these species, the ATom–model agreement is generally good. If anything, the models tend to have too much HOOH. ATom shows systematically large occurrences of low HOOH (50–200 ppt, especially in the central Pacific), indicating, perhaps, that convective or cloud scavenging of HOOH is more effective than is modeled. HCHO shows reasonable agreement in the Atlantic, but in both the central and eastern Pacific, the modeled low end (< 40 ppt) is simply not seen in the ATom data. Also, the models are missing a strong HCHO peak at 300 ppt in the eastern Pacific, probably convection-related, specific to that time period. Thus, in terms of these HO$_x$ precursors, the model climatologies appear to be at least as reactive as the ATom data.

While the ATom-1 data in Fig. 4 are limited to single transects, the model NO$_x$ discrepancies apply across the three tropical regions, and the simple chemical statistics for these flights alone are probably enough to identify measurement–model discrepancies. For the HO$_x$-related species, the models match the first-order statistics from ATom. In terms of using ATom statistics as a model metric, it is encouraging that where some individual models tend to deviate from their peers, they also deviate from the ATom-1 PDs.

4.3.3 Probability densities

Mean profiles do not reflect the heterogeneity seen in Fig. 2, and so we also examine the PDs of the tropical reactivities (Fig. 5). The model PDs (colored lines connecting open circles at the center of each bin) are calculated from the 1 d statistics for mid-August (P2017) using the model blocks shown in Fig. S1. The model grid cells are weighted by air mass and cosine(latitude) and limited to pressures greater than 200 hPa. The ATom PDs (black lines connecting black open circles) are calculated from the 10 s data weighted by (but not averaged over) the number of points in each 10° latitude by 200 hPa pressure bin and then also by cosine (latitude) to compare with the models. In addition, a PD was calculated from the 1° by 200 m average grid-cell values in Fig. 2 (black Xs), and this is also cosine (latitude)-weighted. To check if the high reactivities in the eastern Pacific affected the whole Pacific PD, a separate PD using only central Pacific
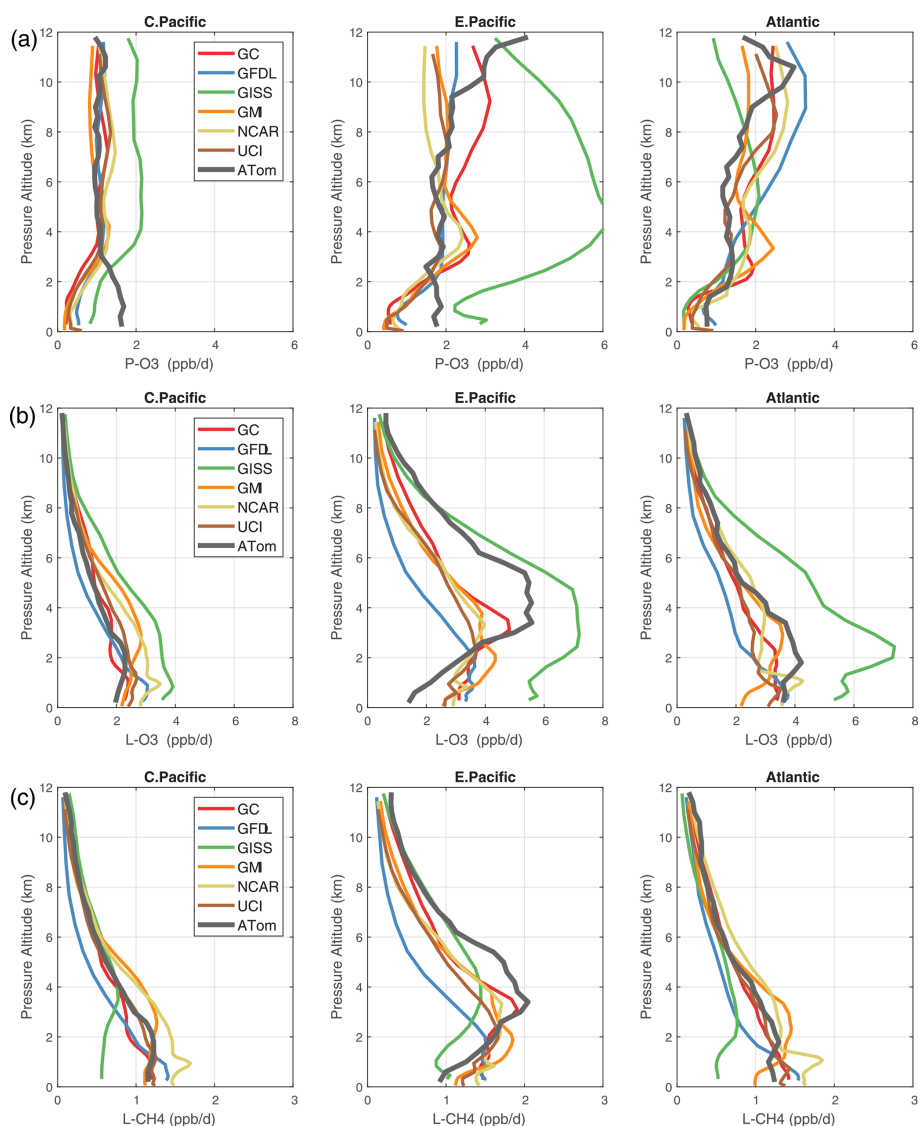
Figure 3. Mean altitude profiles of reactivity (rows: P-O3, L-O3, L-CH4 in ppb d^{-1}) in three domains (columns: C. Pacific, 30° S–30° N by 180–210° E; E. Pacific, 0–30° N by 230–250° E; Atlantic, 30° S–30° N by 326–343° E; ranges are the model blocks). Air parcels are cosine (latitude)-weighted. ATom-1 (gray) results are from Fig. 2, while model results are taken from the August climatologies in Prather et al. (2017).

10 s data was calculated (gray lines connecting open gray circles). The mean reactivities (ppb d^{-1}) from the models and ATom are given in the legend; note that the model values are based on the August climatologies (P2017) and not the MDS-0 values in the table. The "ATom" legend values are the same as in Table 2. The PD binning is shown by the open circles, and occurrences of off-scale reactivities are included in the last point.

For the Pacific (eastern + central, left columns, Fig. 5), the modeled PD climatologies are similar for each of the reactivities (except GISS), and there is fairly good agreement with the ATom-1 PDs. For the Atlantic (right columns, Fig. 5), the models show a larger spread, presumably due to the differ-

ing influence of pollution from neighboring continents. The ATom-1 Atlantic PDs also show slightly larger disagreement with the models (e.g., the maximum in P-O3 at 1–2 ppb d^{-1} and minimum in L-O3 at 2–3 ppb d^{-1}) and the notably higher frequency of hot spots with L-O3 > 5 ppb d^{-1}. The influence of the extreme eastern Pacific reactivities is seen in the statistics generated from the central Pacific values only (CPac; gray circles); e.g., the mean value for L-O3 drops from 1.42 to 1.17 ppb d^{-1}.

The ability to test a model's reactivity statistics with the ATom 10 s data is not obvious, but the PDs based on 1° latitude by 200 m altitude cells (the black Xs) are remarkably close to the PDs based on 2 km (horizontal) by 80 m (vertical)
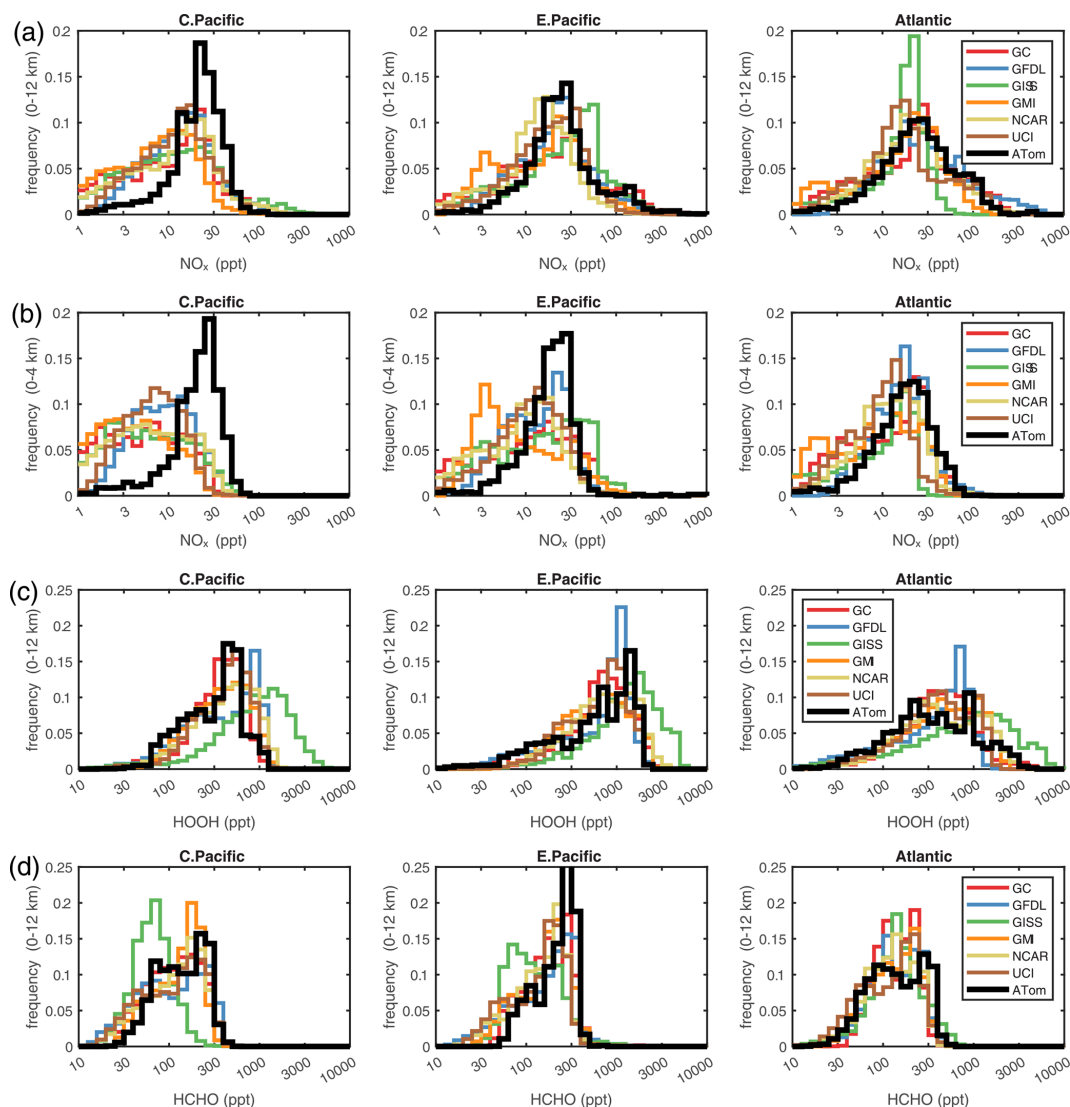
Figure 4. Histograms of probability densities (PDs) of NO_x (0–12 km, **a**), NO_x (0–4 km, **b**), HOOH (0–12 km, **c**), and HCHO (0–12 km, **d**) for the three tropical regions (central Pacific, eastern Pacific, and Atlantic). The ATom-1 data are plotted on top of the six global chemistry models' results for a day in mid-August and sampled as described in Fig. 3.

10 s parcels. With the coarser resolution, we see a slight shift of points from the ends of the PD to the middle as expected, but we find, once again, that the loss in high-frequency, below-model grid-cell resolution is not great. Both ATom-derived PDs more closely resemble each other than any model PD. Thus, current global chemistry models with resolutions of about 100 km by 400 m should be able to capture much of the wide range of chemical heterogeneity in the atmosphere, which for the oceanic transects is, we believe, adequately resolved by the 10 s ATom measurements. Perhaps more surprising, given the different mean profiles in Fig. 3, is that the five model PDs in Fig. 5 look very much alike.

5 Discussion and path forward

5.1 Major findings

This paper opens a door for what the community can do with the ATom measurements and the derived products. ATom's mix of key species allows us to calculate the reactivity of the air parcels and hopefully may become standard for tropospheric chemistry campaigns. We find that the reactivity of the troposphere with respect to O_3 and CH_4 is dominated by a fraction of the air parcels but not by so small and infrequent a fraction as to challenge the ability of current CTMs to simulate these observations and thus be used to study the oxidation budgets. In comparing ATom results with modeled climatologies, we find a systematic ATom–model difference:
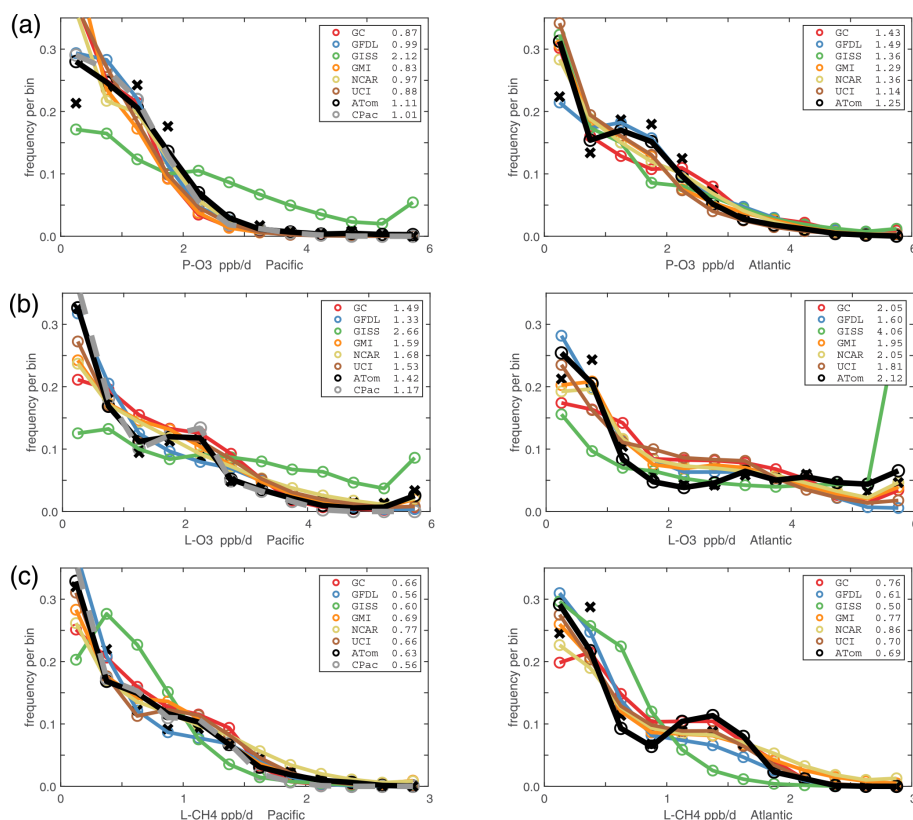
Figure 5. Probability densities (PDs, frequency of occurrence) for the ATom-1 three reactivities (rows: P-O3, L-O3, and L-CH4 in ppb d^{-1}) and for the Pacific and Atlantic from 53° S to 60° N (columns left and right). Each air parcel is weighted as described in the text for equal frequency in large latitude–pressure bins and also by cosine (latitude). The ATom statistics are from the UCIZ model, using MDS-2b and revised RDS* protocol (HNO$_4$ and PAN damping). The Pacific results (solid black) also show the central Pacific alone (dashed gray). The six models' values for a day in mid-August are averaged over longitude for the domains shown in Fig. S1 and then cosine (latitude)-weighted. Mean values (ppb d^{-1}) are shown in the legend. The PD derived from the ATom 10 s parcels binned into 1° latitude by 200 m altitude (as shown for the tropics in Fig. 2) is typical of a high-resolution global model and denoted by black Xs.
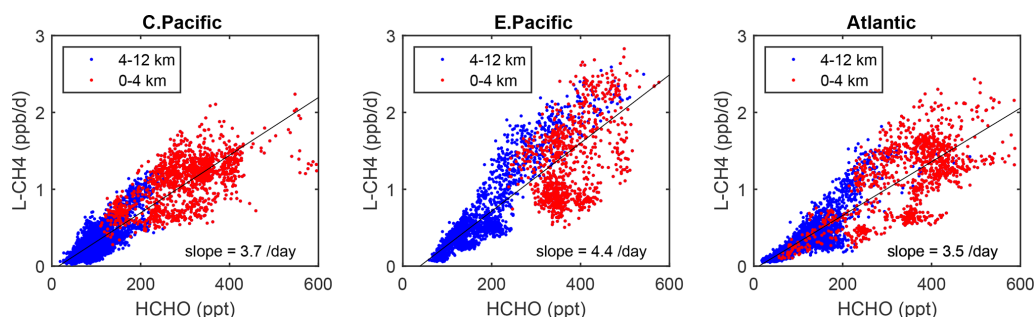
Figure 6. Scatterplot of L-CH4 (ppb d^{-1}) versus HCHO (ppt) for ATom 1 in the three tropical regions shown in Fig. 3. The air parcels are split into the lower troposphere (0–4 km pressure altitude, red dots) where most of the reactivity lies and middle–upper troposphere (4–12 km, blue). A simple linear fit to all data is shown (thin black line), and the slope is given in units of 1 d.

models show a large relative drop in O$_3$ production below 2 km over the tropical oceans, but ATom shows an increase (C.Pac.), no change (E.Pac.), or a much lesser drop (Atl.). We traced this result to the lack of NO$_x$ at 20–60 ppt levels in the

models below 4 km and believe it provides a clear challenge in modeling ozone.

Building our chemical statistics (PDs) from the ATom 10 s air parcels on a scale of 2 km by 80 m, we can identify the fundamental scales of spatial heterogeneity in tropospheric
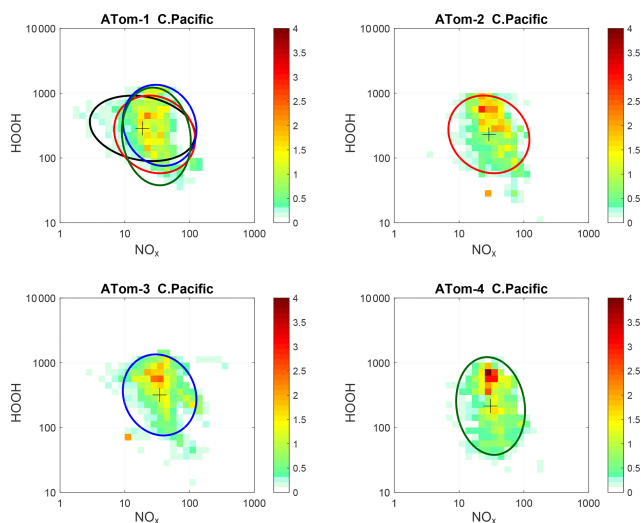
Figure 7. 2D frequency of occurrence (PDs in log ppt mole fraction) of HOOH vs. NO_x for the tropical central Pacific for all four ATom deployments. The cross marks the mean (in log space), and the ellipse is fitted to the rotated PD having the smallest semi-minor axis. The semi-minor and semi-major axes are 2 standard deviations of PD in that direction. The ellipses from ATom-2 (red), ATom-3 (blue), and ATom-4 (dark green) are also plotted in the ATom-1 quadrant.

chemistry. Although heterogeneity occurs at the finest scales (such as seen in some 1 s observations), the majority of variability in terms of the O_3 and CH_4 budgets occurs across scales larger than neighboring 2 km parcels. The PDs measured in ATom can be largely captured by a global model's 100 km by 200 m grid cells in the lower troposphere. This surprising result is evident by comparing the ATom 1D PDs – both species and reactivities – with those from the models' climatologies (Fig. 5). These comparisons show that the modeled PDs are consistent with the innate chemical heterogeneity of the troposphere as measured by the 10 s parcels in ATom. A related conclusion for biomass burning smoke particles is found by Schill et al. (2020), where most of the smoke appears in the background rather than in pollution plumes, and therefore much of the variability occurs on synoptic scales resolved by global models (see their Fig. 1 compared with Fig. 2 here).

5.2 Opportunities and lessons learned

As a quick look at the opportunities provided by the ATom data, we present an example based on the Wolfe et al. (2019) study, which used the F0AM model and semi-analytical arguments to show that troposphere HCHO columns (measurable by satellite and ATom) are related to OH columns (measured by ATom) and thus to CH_4 loss. Figure 6 extends the Wolfe et al. (2019) study using the individual air parcels and plotting L-CH4 (ppb d^{-1}) versus HCHO (ppt) for the three tropical regions where most of the CH_4 loss occurs. The relationship

is linear but with a lot of scatter and has slopes ranging from 3.5 to 4.4 per day over the three tropical regions, but for the largest reactivities (0–4 km, 1–3 ppb d^{-1}), L-CH4 is not so well correlated with HCHO.

As is usual with new model intercomparison projects, we have an opportunity to identify model "features" and identify errors. In the UCI model, an error in the lumped alkane formulation (averaging alkanes C_3H_8 and higher) did not show up in P2018, where UCI supplied all the species, but when the ATom data were used, the UCI model became an outlier. Once found, this problem was readily fixed (hence the current UCIZ model version). Inclusion of the F0AM model with its extensive hydrocarbon oxidation mechanism provided an interesting contrast with the simpler chemistry in the global CCM/CTMs. For a better comparison of the chemical mechanisms, we should have F0AM use 5 d of photolysis fields from one of the CTMs. The anomalous GISS results have been examined by a co-author, but no clear causes have been identified as of this publication. The problem goes beyond just the implementation of the RDS protocol, as it shows up in the model climatology (Figs. 4 and 5, also in P2017).

Decadal-scale shifts in the budgets of O_3 and CH_4 are likely to be evident through the statistical patterns of the key species, rather than simply via average profiles. The underlying design of ATom was to collect enough data to develop such a multivariate chemical climatology. As a quick look across the four deployments, we show the joint 2D PDs on a logarithmic scale as in P2017 for HOOH versus NO_x in Fig. 7. The patterns for the tropical central Pacific are quite similar for the four seasons of ATom deployments, and the fitted ellipses are almost identical for ATom 2, 3, and 4. Thus, for these species in the central Pacific, we believe that ATom provides a benchmark of the 2016–2018 chemical state, one that can be revisited with an aircraft mission in a decade to detect changes in not only chemical composition, but also reactivity.

ATom identifies which "highly reactive" spatial or chemical environments could be targeted in future campaigns for process studies or to provide a better link between satellite observations and photochemical reactivity (e.g., eastern Pacific mid-troposphere in August, Fig. 2). The many corollary species measured by ATom (not directly involved in CH_4 and O_3 chemistry) can provide clues to the origin or chemical processing of these environments. We hope to engage a wider modeling community beyond the ATom science team, as in H2018, in the calculation of photochemical processes, budgets, and feedbacks based on all four ATom deployments.

and permanently on Dryad|UCI (https://doi.org/10.7280/D1B12H; Prather, 2022). This publication marks the public release of the reactivity calculations for ATom 2, 3, and 4, but we have not yet analyzed these data, and thus users should be aware and report any anomalous features to the lead authors via haog2@uci.edu and mprather@uci.edu. Details of the ATom mission and data sets are found on the NASA mission website (https://espo.nasa.gov/atom/content/ATom) and in the final archive at Oak Ridge National Laboratory (ORNL; https://daac.ornl.gov/ATOM/guides/ATom_merge.html, last access: 12 December 2022; https://doi.org/10.3334/ORNLDAAC/1581, Wofsy et al., 2018). The MATLAB scripts and data sets used in the analysis here are posted on Dryad (https://doi.org/10.7280/D1Q699; Guo, 2021).

References

Burkholder, J. B., Sander, S. P., Abbatt, J. P. D., Barker, J. R., Huie, R. E., Kolb, C. E., Kurylo, M. J., Orkin, V. L., Wilmouth, D. M., and Wine, P. H.: Chemical kinetics and photochemical data for use in atmospheric studies: evaluation number 18, Pasadena, CA, Jet Propulsion Laboratory, National Aeronautics and Space Administration, http://hdl.handle.net/2014/45510 (last access: 13 September 2021), 2015.

Charlton-Perez, C. L., Evans, M. J., Marsham, J. H., and Esler, J. G.: The impact of resolution on ship plume simulations with NO_x chemistry, Atmos. Chem. Phys., 9, 7505–7518, https://doi.org/10.5194/acp-9-7505-2009, 2009.

Douglass, A. R., Prather, M. J., Hall, T. M., Strahan, S. E., Rasch, P. J., Sparling, L. C., Coy, L., and Rodriguez, J. M.: Choosing meteorological input for the global modeling initiative assessment of high-speed aircraft, J. Geophys. Res.-Atmos., 104, 27545–27564, https://doi.org/10.1029/1999JD900827, 1999.

Eastham, S. D. and Jacob, D. J.: Limits on the ability of global Eulerian models to resolve intercontinental transport of chemical plumes, Atmos. Chem. Phys., 17, 2543–2553, https://doi.org/10.5194/acp-17-2543-2017, 2017.

Griffiths, P. T., Murray, L. T., Zeng, G., Shin, Y. M., Abraham, N. L., Archibald, A. T., Deushi, M., Emmons, L. K., Galbally, I. E., Hassler, B., Horowitz, L. W., Keeble, J., Liu, J., Moeini, O., Naik, V., O'Connor, F. M., Oshima, N., Tarasick, D., Tilmes, S., Turnock, S. T., Wild, O., Young, P. J., and Zanis, P.: Tropospheric ozone in CMIP6 simulations, Atmos. Chem. Phys., 21, 4187–4218, https://doi.org/10.5194/acp-21-4187-2021, 2021.

Guo, H.: Heterogeneity and chemical reactivity of the remote Troposphere defined by aircraft measurements, Dryad [data set], https://doi.org/10.7280/D1Q699, 2021.

Hall, S. R., Ullmann, K., Prather, M. J., Flynn, C. M., Murray, L. T., Fiore, A. M., Correa, G., Strode, S. A., Steenrod, S. D., Lamarque, J.-F., Guth, J., Josse, B., Flemming, J., Huijnen, V., Abraham, N. L., and Archibald, A. T.: Cloud impacts on photochemistry: building a climatology of photolysis rates from the Atmospheric Tomography mission, Atmos. Chem. Phys., 18, 16809–16828, https://doi.org/10.5194/acp-18-16809-2018, 2018.

Heald, C. L., Coe, H., Jimenez, J. L., Weber, R. J., Bahreini, R., Middlebrook, A. M., Russell, L. M., Jolleys, M., Fu, T.-M., Allan, J. D., Bower, K. N., Capes, G., Crosier, J., Morgan, W. T., Robinson, N. H., Williams, P. I., Cubison, M. J., DeCarlo, P. F., and Dunlea, E. J.: Exploring the vertical profile of atmospheric organic aerosol: comparing 17 aircraft field campaigns with a global model, Atmos. Chem. Phys., 11, 12673–12696, https://doi.org/10.5194/acp-11-12673-2011, 2011.

Myhre, G., Shindell, D., and Pongratz, J.: Anthropogenic and Natural Radiative Forcing, in: Climate Change 2013: The Physical Science Basis, IPCC WGI Contribution to the Fifth Assessment Report, Cambridge University Press, 659–740, https://doi.org/10.1017/CBO9781107415324.018, 2014.

Naik, V., Voulgarakis, A., Fiore, A. M., Horowitz, L. W., Lamarque, J.-F., Lin, M., Prather, M. J., Young, P. J., Bergmann, D., Cameron-Smith, P. J., Cionni, I., Collins, W. J., Dalsøren, S. B., Doherty, R., Eyring, V., Faluvegi, G., Folberth, G. A., Josse, B., Lee, Y. H., MacKenzie, I. A., Nagashima, T., van Noije, T. P. C., Plummer, D. A., Righi, M., Rumbold, S. T., Skeie, R., Shindell, D. T., Stevenson, D. S., Strode, S., Sudo, K., Szopa, S., and Zeng,

G.: Preindustrial to present-day changes in tropospheric hydroxyl radical and methane lifetime from the Atmospheric Chemistry and Climate Model Intercomparison Project (ACCMIP), Atmos. Chem. Phys., 13, 5277–5298, https://doi.org/10.5194/acp-13-5277-2013, 2013.

Prather, M.: NASA Atmospheric Tomography Mission: Modeling and reactivity data sets, Dryad [data set], https://doi.org/10.7280/D1B12H, 2022.

Prather, M. J., Ehhalt, D., Dentener, F., Derwent, R., Dlugokencky, E. J., Holland, E., Isaksen, I., Katima, J., Kirchhoff, V., Matson, P., and Midgley, P.: Chapter 4 – Atmospheric Chemistry and Greenhouse Gases, Climate Change 2001: The Scientific Basis, Third Assessment Report of the Intergovernmental Panel on Climate Change, 239–287, Cambridge University Press, Cambridge UK, ISBN 0521014956, 2001.

Prather, M. J., Zhu, X., Flynn, C. M., Strode, S. A., Rodriguez, J. M., Steenrod, S. D., Liu, J., Lamarque, J.-F., Fiore, A. M., Horowitz, L. W., Mao, J., Murray, L. T., Shindell, D. T., and Wofsy, S. C.: Global atmospheric chemistry – which air matters, Atmos. Chem. Phys., 17, 9081–9102, https://doi.org/10.5194/acp-17-9081-2017, 2017.

Prather, M. J., Flynn, C. M., Zhu, X., Steenrod, S. D., Strode, S. A., Fiore, A. M., Correa, G., Murray, L. T., and Lamarque, J.-F.: How well can global chemistry models calculate the reactivity of short-lived greenhouse gases in the remote troposphere, knowing the chemical composition, Atmos. Meas. Tech., 11, 2653–2668, https://doi.org/10.5194/amt-11-2653-2018, 2018.

Rastigejev, Y., Park, R., Brenner, M. P., and Jacob, D. J.: Resolving intercontinental pollution plumes in global models of atmospheric transport, J. Geophys. Res.-Atmos., 115, D012568, https://doi.org/10.1029/2009JD012568, 2010.

Schill, G. P., Froyd, K. D., Bian, H., Kupc, A., Williamson, C., Brock, C. A., Ray, E., Hornbrook, R. S., Hills, A. J., Apel, E. C., and Chin, M.: Widespread biomass burning smoke throughout the remote troposphere, Nat. Geosci., 13, 422–427, https://doi.org/10.1038/s41561-020-0586-1, 2020.

Science team of the NASA Atmospheric Tomography Mission: ATom, NASA [data set], https://espo.nasa.gov/atom/content/ATom, last access: 13 September 2021.

Stevenson, D. S., Dentener, F. J., Schultz, M. G., Ellingsen, K., Van Noije, T. P. C., Wild, O., Zeng, G., Amann, M., Atherton, C. S., Bell, N., and Bergmann, D. J.: Multimodel ensemble simulations of present-day and near-future tropospheric ozone, J. Geophys. Res.-Atmos., 111, D006338, https://doi.org/10.1029/2005JD006338, 2006.

Stevenson, D. S., Young, P. J., Naik, V., Lamarque, J.-F., Shindell, D. T., Voulgarakis, A., Skeie, R. B., Dalsoren, S. B., Myhre, G., Berntsen, T. K., Folberth, G. A., Rumbold, S. T., Collins, W. J., MacKenzie, I. A., Doherty, R. M., Zeng, G., van Noije, T. P. C., Strunk, A., Bergmann, D., Cameron-Smith, P., Plummer, D. A., Strode, S. A., Horowitz, L., Lee, Y. H., Szopa, S., Sudo, K., Nagashima, T., Josse, B., Cionni, I., Righi, M., Eyring, V., Conley, A., Bowman, K. W., Wild, O., and Archibald, A.: Tropospheric ozone changes, radiative forcing and attribution to emissions in the Atmospheric Chemistry and Climate Model Intercomparison Project (ACCMIP), Atmos. Chem. Phys., 13, 3063–3085, https://doi.org/10.5194/acp-13-3063-2013, 2013.

Stevenson, D. S., Zhao, A., Naik, V., O'Connor, F. M., Tilmes, S., Zeng, G., Murray, L. T., Collins, W. J., Griffiths, P. T., Shim, S., Horowitz, L. W., Sentman, L. T., and Emmons, L.: Trends in global tropospheric hydroxyl radical and methane lifetime since 1850 from AerChemMIP, Atmos. Chem. Phys., 20, 12905–12920, https://doi.org/10.5194/acp-20-12905-2020, 2020.

Stocker, T. F., Qin, D., Plattner, G. K., Tignor, M., Allen, S. K., Boschung, J., Nauels, A., Xia, Y., Bex, V., and Midgley, P. M.: Contribution of working group I to the fifth assessment report of the intergovernmental panel on climate change, Cambridge University Press, 33–115, ISBN 978-1-107-66182-0, 2013.

Tie, X., Brasseur, G., and Ying, Z.: Impact of model resolution on chemical ozone formation in Mexico City: application of the WRF-Chem model, Atmos. Chem. Phys., 10, 8983–8995, https://doi.org/10.5194/acp-10-8983-2010, 2010.

Voulgarakis, A., Naik, V., Lamarque, J.-F., Shindell, D. T., Young, P. J., Prather, M. J., Wild, O., Field, R. D., Bergmann, D., Cameron-Smith, P., Cionni, I., Collins, W. J., Dalsøren, S. B., Doherty, R. M., Eyring, V., Faluvegi, G., Folberth, G. A., Horowitz, L. W., Josse, B., MacKenzie, I. A., Nagashima, T., Plummer, D. A., Righi, M., Rumbold, S. T., Stevenson, D. S., Strode, S. A., Sudo, K., Szopa, S., and Zeng, G.: Analysis of present day and future OH and methane lifetime in the ACCMIP simulations, Atmos. Chem. Phys., 13, 2563–2587, https://doi.org/10.5194/acp-13-2563-2013, 2013.

Wofsy, S. C.: HIAPER Pole-to-Pole Observations (HIPPO): fine-grained, global-scale measurements of climatically important atmospheric gases and aerosols, Philos. T. Roy. Soc. A, 369, 2073–2086, https://doi.org/10.1098/rsta.2010.0313, 2011.

Wofsy, S. C., Afshar, S., Allen, H. M., Apel, E. C., Asher, E. C., Barletta, B., Bent, J., Bian, H., Biggs, B. C., Blake, D. R., Blake, N., Bourgeois, I., Brock, C. A., Brune, W. H., Budney, J. W., Bui, T. P., Butler, A., Campuzano-Jost, P., Chang, C.S., Chin, M., Commane, R., Correa, G., Crounse, J. D., Cullis, P. D., Daube, B.C., Day, D. A., Dean-Day, J. M., Dibb, J. E., DiGangi, J. P., Diskin, G. S., Dollner, M., Elkins, J. W., Erdesz, F., Fiore, A. M., Flynn, C. M., Froyd, K. D., Gesler, D. W., Hall, S. R., Hanisco, T. F., Hannun, R. A., Hills, A. J., Hintsa, E. J., Hoffman, A., Hornbrook, R. S., Huey, L. G., Hughes, S., Jimenez, J. L., Johnson, B. J., Katich, J. M., Keeling, R. F., Kim, M. J., Kupc, A., Lait, L. R., Lamarque, J.-F., Liu, J., McKain, K., Mclaughlin, R. J., Meinardi, S., Miller, D. O., Montzka, S. A, Moore, F. L., Morgan, E. J., Murphy, D. M., Murray, L. T., Nault, B. A., Neuman, J. A., Newman, P. A., Nicely, J. M., Pan, X., Paplawsky, W., Peischl, J., Prather, M. J., Price, D. J., Ray, E. A., Reeves, J. M., Richardson, M., Rollins, A. W., Rosenlof, K. H., Ryerson, T. B., Scheuer, E., Schill, G. P., Schroder, J. C., Schwarz, J. P., St.Clair, J. M., Steenrod, S. D., Stephens, B. B., Strode, S. A., Sweeney, C., Tanner, D., Teng, A. P., Thames, A. B., Thompson, C. R., Ullmann, K., Veres, P. R., Vieznor, N., Wagner, N. L., Watt, A., Weber, R., Weinzierl, B., Wennberg, P. O., Williamson, C. J., Wilson, J. C., Wolfe, G. M., Woods, C. T., and Zeng L. H.: ATom: Merged Atmospheric Chemistry, Trace Gases, and Aerosols, ORNL DAAC [data set], Oak Ridge, Tennessee, USA, https://doi.org/10.3334/ORNLDAAC/1581, https://daac.ornl.gov/ATOM/guides/ATom_merge.html (last access: 12 December 2022), 2018.

Wolfe, G. M., Nicely, J. M., Clair, J. M. S., Hanisco, T. F., Liao, J., Oman, L. D., Brune, W. B., Miller, D., Thames, A., Abad, G. G., and Ryerson, T. B.: Mapping hydroxyl variability throughout the global remote troposphere via synthesis of airborne and satel-

lite formaldehyde observations, P. Natl. Acad. Sci. USA, 116, 11171–11180, https://doi.org/10.1073/pnas.1821661116, 2019.

Young, P. J., Archibald, A. T., Bowman, K. W., Lamarque, J.-F., Naik, V., Stevenson, D. S., Tilmes, S., Voulgarakis, A., Wild, O., Bergmann, D., Cameron-Smith, P., Cionni, I., Collins, W. J., Dalsøren, S. B., Doherty, R. M., Eyring, V., Faluvegi, G., Horowitz, L. W., Josse, B., Lee, Y. H., MacKenzie, I. A., Nagashima, T., Plummer, D. A., Righi, M., Rumbold, S. T., Skeie, R. B., Shindell, D. T., Strode, S. A., Sudo, K., Szopa, S., and Zeng, G.: Pre-industrial to end 21st century projections of tropospheric ozone from the Atmospheric Chemistry and Climate Model Intercomparison Project (ACCMIP), Atmos. Chem. Phys., 13, 2063–2090, https://doi.org/10.5194/acp-13-2063-2013, 2013.

Young, P. J., Naik, V., Fiore, A. M., Gaudel, A., Guo, J., Lin, M. Y., Neu, J. L., Parrish, D. D., Rieder, H. E., Schnell, J. L., and Tilmes, S.: Tropospheric Ozone Assessment Report: Assessment of global-scale model performance for global and regional ozone distributions, variability, and trends, Elementa, 6, 10, https://doi.org/10.1525/elementa.265, 2018.

Yu, K., Jacob, D. J., Fisher, J. A., Kim, P. S., Marais, E. A., Miller, C. C., Travis, K. R., Zhu, L., Yantosca, R. M., Sulprizio, M. P., Cohen, R. C., Dibb, J. E., Fried, A., Mikoviny, T., Ryerson, T. B., Wennberg, P. O., and Wisthaler, A.: Sensitivity to grid resolution in the ability of a chemical transport model to simulate observed oxidant chemistry under high-isoprene conditions, Atmos. Chem. Phys., 16, 4369–4378, https://doi.org/10.5194/acp-16-4369-2016, 2016.

Zhuang, J., Jacob, D. J., and Eastham, S. D.: The importance of vertical resolution in the free troposphere for modeling intercontinental plumes, Atmos. Chem. Phys., 18, 6039–6055, https://doi.org/10.5194/acp-18-6039-2018, 2018.